A Reduced Order Model for the Stable LC-Filter Design on Shipboard DC Microgrids

Andrea Alessia Tavagnutti
Dept. of Engineering and Architecture
University of Trieste
Trieste, Italy
andreaalessia.tavagnutti@phd.units.it

Daniele Bosich
Dept. of Engineering and Architecture
University of Trieste
Trieste, Italy
dbosich@units.it

Stefano Pastore
Dept. of Engineering and Architecture
University of Trieste
Trieste, Italy
pastore@units.it

Giorgio Sulligoi
Dept. of Engineering and Architecture
University of Trieste
Trieste, Italy
gsulligoi@units.it

***Abstract*—In advanced ships, the power request is increasing as most of the loads, including propulsion, are electrically supplied. This aspect represents a challenge when focusing on the dynamics performance in balancing the power flows and when considering the large amount of energy to be managed. To this issue, the DC technology is an effective solution to prioritize the flexibility of shipboard power systems and for a better use of onboard energy. A DC shipboard microgrid is a complex system, incorporating several controlled converters. Between the main priorities, certainly the system stability has a prominent role. Indeed, unstable interactions among controlled converters and their filtering stages can arise during the ship operation, thus eventually compromising the ship mission. As the analytical stability assessment on this controlled system is not feasible, then equivalent models or order reductions help when investigating on stability performance. In this work, a cascade-connected shipboard DC system is studied, and an analytical expression of its stability boundaries is attained. The stability results are verified by means of circuital simulations to identify when the load filters are negligible, then achieving the chased order reduction.**

Keywords—small-signal stability, DC microgrids, DC-DC converters, LC filters.

I. Introduction

To achieve a green maritime transportation, the vessels designers are addressed towards reduction in emissions and fuel consumption [1]-[2]. One of the technological vectors for such a change is represented by the All-Electric Ship (AES) concept [3], meaning that all the onboard loads are powered from electric energy. The actual standard for such power systems in based on AC distributions. Nonetheless, the adoption of the Medium Voltage Direct Current (MVDC) technology represents the future to maximize both flexibility and efficiency of marine systems [4]. In an MVDC power system, the most important elements are definitely the power electronics interfaces, that serve as conversion stages. They enable the full controllability of the shipboard system and help during the fault management process [5]. On one hand, such converters are provided of input/output filters to ensure power quality requirements [6], on the other they are usually tightly controlled for dynamics reasons. If during the design phase on converters the choices on filters and control bandwidths are not integrated, harmful interactions can be triggered during operation, even resulting in system instability [7]. This issue is largely debated in literature [8]-[10] since an unstable behavior definitely determines a ship blackout. Indeed, the Std. 1709 [11] recommends the steps to verify the shipboard power system stability during the design phase. However, the analytical identification of the stability boundaries of a DC power grid is a complex task also for relatively simple systems. The perfect example is the cascade-connection of generating and load converters. With appropriate hypotheses, this system is studied in previous works [12]-[13] as a fifth-order model, later simplified by neglecting the load converter filter. Thus, a third-order model is obtained to get analytical expressions for the stability boundary of the cascade-connected system. Albeit the third-order hypothesis is debated [12] and exploited [13]-[15] in previous papers, the analytical expression of its applicability area has not been defined yet. This paper fills this gap by deriving the analytical expression of the fifth-order model stability boundary. This is made possible thanks to an extension of the Routh-Hurwitz (R-H) theorem. The fifth and third-order stability conditions are visually contrasted in terms of dynamics performance and power quality. The results are then verified through numerical simulations on Matlab/Simulink and on Typhoon HIL.

II. Cascade-Connected Shipboard DC Microgrid

A cascade-connected shipboard DC power grid is the case study. This simple configuration can be representative of the converters included in a single zone or can be considered as the equivalent of a more complex radial distribution with multiple load and generating converters.

A. Fifth and third-order model

The goal is to obtain the analytical expression of the small-signal stability boundaries for a cascade-connected DC system (Fig. 1). These results will be then compared with the ones valid for a reduced-order model, depicted in Fig. 2. The power system is a cascade connection of two DC-DC buck converters, a generating (converter 1) and a load one (converter 2). Both voltage-controlled converters are provided of RLC output filters, designed to meet the power quality requirements [11]. The focus is on load converter control bandwidth, thus the converter 1 is modeled as an E constant voltage source. The load converter control (i.e. ω_2 is the bandwidth) is conversely modeled by a pure integral regulator, whose gain is $Ki=\omega_2/V_{1ref}$ [14]. The converter 2 regulates the ratio $D_2=V_2/V_1$ between generating voltage V_1 and load voltage V_2, with the dynamics imposed by the ω_2 converter control bandwidth.

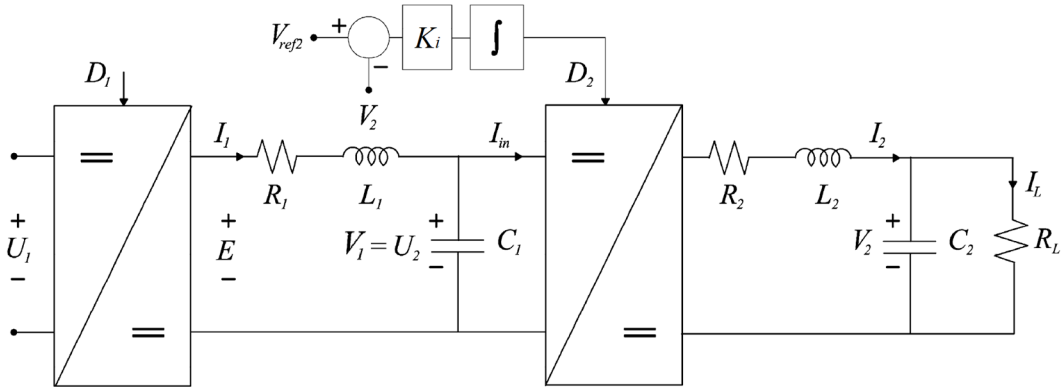

Fig. 1. Complete order cascade-connected MVDC power system [12].

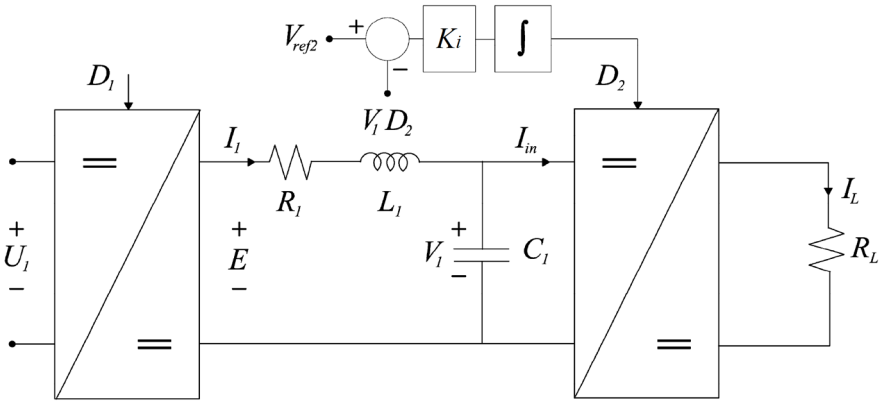

Fig. 2. Reduced-order cascade-connected MVDC power system [12].

The fifth-order system is modeled by neglecting the switching behavior of the power converter, thus (1) are representative of an Average Value Model (AVM) for the power grid in Fig. 1. In those equations, the subscript 1 identifies the generating converter, while the subscript 2 the load one. The supplied load is modeled by a resistance R_L.

$$\begin{cases} \frac{dI_1}{dt} = -\frac{R_1 I_1}{L_1} - \frac{V_1}{L_1} + \frac{E}{L_1} \\ \frac{dV_1}{dt} = \frac{I_1}{C_1} - \frac{D_2 I_2}{C_1} \\ \frac{dI_2}{dt} = \frac{D_2 V_1}{L_2} - \frac{R_2 I_2}{L_2} - \frac{V_2}{L_2} \\ \frac{dV_2}{dt} = \frac{I_2}{C_2} - \frac{V_2}{R_L C_2} \\ \frac{dD_2}{dt} = -K_i V_2 + K_i V_{ref2} \end{cases} \quad (1)$$

The fifth-order model described by previous equations can be further simplified to a third-order model. This becomes possible only if the condition $\omega_2 \prec\prec \omega_{f2}$ is verified [12], where $\omega_{f2}=1/\sqrt{L_2 C_2}$ is the load converter resonance frequency. The modeling hypotheses discussed in [12] make it possible to neglect the load converter filter, thus obtaining a third-order AVM as in Fig. 2. The related equations are simplified as in (2).

$$\begin{cases} \frac{dI_1}{dt} = -\frac{R_1 I_1}{L_1} - \frac{V_1}{L_1} + \frac{E}{L_1} \\ \frac{dV_1}{dt} = \frac{I_1}{C_1} - \frac{V_1 D_2^2}{R_L C_1} \\ \frac{dD_2}{dt} = -K_i V_1 D_2 + K_i V_{2ref} \end{cases} \quad (2)$$

B. *Filters design*

As in [12]-[13], a test case is proposed to study the relation between stability performance and parameters on load filtering stages. These results can be further extended by using data of a real shipboard DC power system. The RLC filters parameters for the generating converter are defined by the power quality requirements, and they are not changed during the whole study. Instead, the load converters filters will be calibrated to discuss about the small-signal stability of the DC system. The main requirements of the two cascade-connected converters are given in Table I. The converter power and the inductor current are identified respectively as P_{nk} and I_{nk}. The ratio between V_{nk} output and U_{nk} input voltage is defined as D_{nk} duty, and the switching frequency as f_{sk}. Once chosen the power quality requirements ($\Delta V_{\%k}$ voltage and $\Delta I_{\%k}$ current ripple, $\Delta P_{\%k}$ percentage of losses), (3)-(4) are adopted to calculate the filters values. By this design procedure, the converter 1 filter values are R_1=0.014 Ω, C_1=1.8 mF and L_1=50 μH. Conversely, the second filter is the goal of the study, both $\Delta V_{\%2}$ and $\Delta I_{\%2}$ are indeed not defined at this stage.

TABLE I. Converters requirements.

	Converter 1	Converter 2
P_{nk} [MW]	8.0	6.0
U_{nk} [V]	1630	1500
V_{nk} [V]	1500	1000
D_{nk}	0.92	0.67
I_{nk} [A]	5333	6000
f_{sk} [Hz]	1500	3000
$\Delta P_{\%k}$	0.05	0.03
$\Delta V_{\%k}$	0.05	-
$\Delta I_{\%k}$	0.3	-

$$\begin{cases} D_{nk} = \frac{V_{nk}}{U_{nk}} \\ I_{nk} = \frac{P_{nk} - \Delta P_{\%k} P_{nk}}{V_{nk}} \end{cases} \quad (3) \qquad \begin{cases} R_k = \frac{\Delta P_{\%k} P_{nk}}{I_{nk}^2} \\ L_k = \frac{(U_{nk} - V_{nk}) D_{nk}}{f_{sk} I_{nk} \Delta I_{\%k}} \\ C_k = \frac{1 - D_{nk}}{8 L_k f_{sk}^2 \Delta V_{\%k}} \end{cases} \quad (4)$$

III. Small-Signal Stability Analysis

In previous works, the decision to neglect the load converter filter (under appropriate hypotheses) has greatly simplified the small signal stability study on controlled DC power grids [12], [13], [15]. Additionally, this assumption also allows the load converters aggregation [14]. However, this third-order hypothesis has an applicability limit. This work wants to find it, basing on the analytical definition of the stability boundary for the fifth-order model. The latter behaves strictly closer to the real controlled DC system, thus it constitutes the benchmark for later validate the third-order model. The fifth-order model analytical stability boundary is achievable thanks to the application of the R-H criterion.

A. Stability boundaries

To obtain the small-signal stability condition for the two models, (1)-(2) are linearized around the operating points while applying the Laplace transformation. The admittance Y_{in1} at the output of converter 1 and the total impedance Z_t are thus obtained by neglecting the filter resistances. The study starts with the third-order model, where Y_{in1} is in (5) and Y_t is the inverse of (6). Now the equation $DenY_t(s)=0$ can be solved in ω_2, whose result is the maximum-admissible load converter control bandwidth (i.e. ω_{2max}) to ensure the small-signal stability of third-order model (7).

$$\bar{Y}_{in1} = \frac{\widetilde{I_{in}}}{\widetilde{V_1}} = \frac{D_{20}^2 (s+\omega_2)}{R_L (s+\omega_2)} \quad (5)$$

$$\bar{Z}_t = sL_1 + (sC_1 + \bar{Y}_{in1})^{-1} \quad (6)$$

$$\omega_{2\max} = \frac{-L_1 D_2^2 + \sqrt{L_1^2 D_2^4 + 4 R_L^2 L_1 C_1}}{2 L_1 C_1 R_L} \quad (7)$$

The same analysis can be performed on the fifth-order model. The Y_{in1} admittance at the output of converter 1 is in (8), whereas the total impedance Z_t is again calculated in (6). The denominator of $Y_t(s)=I_1(s)/E(s)$ admittance at the output of the generating converter 1 (Fig. 1) is defined in (A1), and then simplified as in (A2). In order to investigate the system stability, the R-H criterion is then applied to (A2). First of all, the degree of (A2) is lowered from fifth to third using an appropriate formulation (the details are in appendix). The result is again a third-order expression (9)

$$\bar{Y}_{in1} = \frac{\widetilde{I_{in}}}{\widetilde{V_1}} = \frac{D_{20}^2 (R_L C_2 s^2 + s - \omega_2)}{L_2 C_2 R_L s^3 + L_2 s^2 + R_L s + R_L \omega_2} \quad (8)$$

$$a_0 x^3 + a_1 x^2 + a_2 x + a_3 = 0 \quad (9)$$

In order to guarantee the system stability, the R-H criterion states that all the a_i coefficients and the $b_i=a_1a_2-a_0a_3$ one must be positive. This results in the conditions (10)-(13):

$$a_0 = \frac{1 - C_2 R_L \omega_2}{L_2 C_2} > 0, \ \ if \ C_2 < \frac{1}{R_L \omega_2} \quad (10)$$

$$a_1 = \frac{-D_2^2 \omega_2}{C_1 C_2 R_L^2 (C_2 R_L \omega_2 - 1)} + \frac{D_2^2 + R_L \omega_2 C_1}{C_1 R_L C_2 L_2} > 0, if \ C_2 < \frac{1}{R_L \omega_2} \quad (11)$$

$$a_2 = \frac{R_L - R_L^2 \omega_2 C_2 - L_1 D_2^2 \omega_2}{L_1 C_1 R_L L_2 C_2} > 0, \ \ if \ C_2 < \frac{1}{R_L \omega_2} - \frac{L_1 D_2^2}{R_L^2} \quad (12)$$

$$a_3 = \frac{\omega_2}{L_1 C_1 L_2 C_2} > 0, \ \ if \ \omega_2 > 0 \quad (13)$$

The condition (13) is always guaranteed, while among the other three the most stringent is the (12). The last condition to check is the one on b_i, which results in (14). The complete expression of the $C_2^{\pm}$ is given in (A5).

$$-D_2^2 R_L^4 \omega_2^2 (C_2 - C_2^+)(C_2 - C_2^-) \geq 0 \quad (14a)$$

$$C_2 < C_2^- \ and \ C_2 > C_2^+ \quad (14b)$$

If (12) is satisfied, the curves $C_2^{\pm}$ in the ω_2-C_2 plane represent the stability limits for the cascade-connected DC system. All the previous equations describe the stability for the complete fifth-order model. Among all the above-mentioned conditions, only the $C_2<C_2^-$ sets an actual boundary, which will be explained later in the Section. To provide a complete overview on the complex fifth-order model, it is interesting to show how this boundary moves (Fig. 3) as the fixed values of L_2 changes. In particular, if L_2 is short-circuited, the obtained blue curve is an absolute inferior limit. Therefore, if the capacitance/bandwidth cross stays below the blue line, the system stability is certainly guaranteed whichever the value of L_2.

B. Power quality and stability performance

By replacing the C_2 and L_2 with $\Delta V_{\%}$ and $\Delta I_{\%}$ (4), it is possible to obtain all the expressions (10)-(14) as functions of power quality indices on load. If both voltage and current ripple play as variables, the surface in Fig. 4 is thus consequent, in which the stable combination of operating points lays above the surface. When a specific value of current ripple is set, the graph in the ω_2–$\Delta V_{\%}$ plane is the result, as in Fig. 5 with $\Delta I_{\%}$=0.2. In such a graph, the stability limit for the third-order model (7) is given by the green line. While the stability limit for fifth-order model is determined by observing the relative location on blue-red curves. Particularly, the stable region for the fifth-order model is above the ΔV_2^- red curve and below the ΔV_2^+ blue

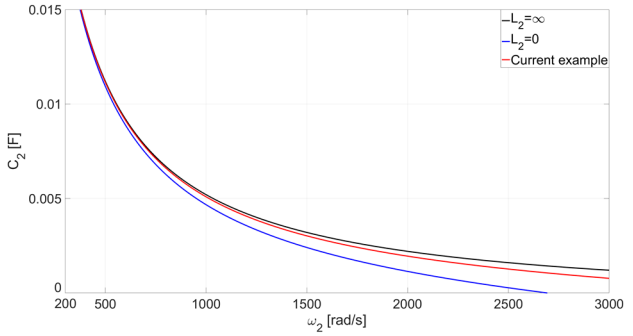

Fig. 3. $C_2^-=f(\omega_2)$ for different L_2 values. The red curve (current example) refers to a $\Delta I_{\%}$ value of 0.2.

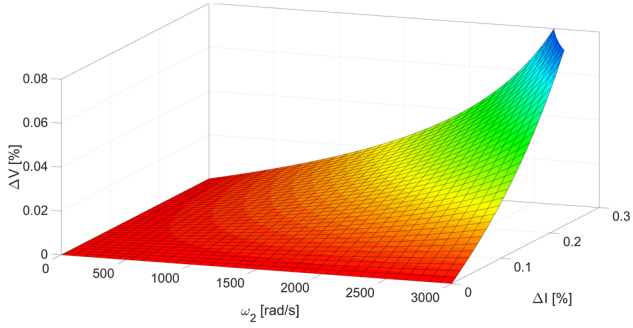

Fig. 4. 3-D graph representing the stability boundary in terms of power quality requirements and control bandwidth.

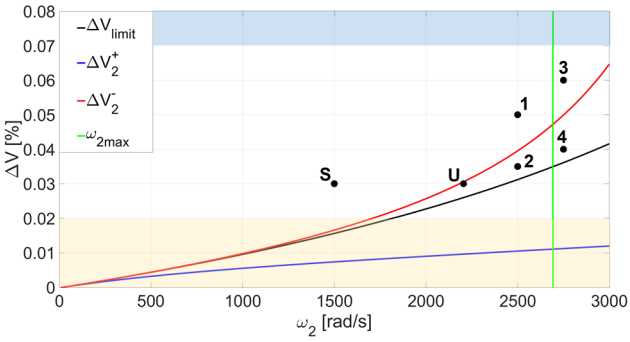

Fig. 5. Stability conditions on the ω_2-$\Delta V_{\%}$ plane.

one. As also the condition (12) must be verified, the admissible values are the ones above the ΔV_{limit} black curve. This consideration allows to recognize the only ω_2-ΔV points above the red curve as stable cross for the fifth-order model. In the admissible-stable area in Fig. 5, other zones are to be excluded for system design reasons on voltage ripple. The colored areas depict minimum-maximum limits for voltage ripple choices in the filter capacitance design. For example, the yellow area should be avoided as the related $\Delta V_{\%}$ are too small, thus unfeasible in a real design. Then, also the blue area is not doable, as characterized by voltage ripple values that are not in accordance with the requirements of Std. [11]. On the relative positions of third/fifth order limits in Fig. 5, a conclusion is consequent. On one hand, the stability study on third-order model is quite basic, thus feasible solutions are at hand especially when the control bandwidth is not that high. On the other, the fifth-order (complex) model can provide stable designs, also when pursuing high-bandwidths solutions.

IV. Validation of Stability Analysis

The outcomes of stability analysis are validated in this Section with numerical simulations, performed both on Simulink and on Typhoon HIL high-performance platform.

A. *System configuration*

Firstly, Average Value Models (AVM) are developed in Simulink. To this purpose, the fifth-order model is developed as in (1), while the third order model comes from (2). On the other hand, the Typhoon implementation is a circuital one, including the switching phenomenon of the power converters. For the following test, the $\Delta I_{\%}$ is set at 0.2, while the values of $\Delta V_{\%}$ and ω_2 are modified to illustrate the behavior of the controlled DC grid. Once $\Delta I_{\%}$ is imposed and the curves are obtained (Fig. 5), the stable region for the fifth order model is above the red line, while the stable region of the third-order model is on the left of green line. The DC system starts to work from an initial condition on bus capacitor voltage, which is set at 95% of its rated value. This small perturbation on voltage forces the consequent dynamic transient towards the final equilibrium condition.

B. *Dynamics tests for stability confirmation*

Four points are chosen in the Fig. 5 (i.e. numbers) to investigate the behavior of AVMs. This study wants to emphasize the areas of ω_2-$\Delta V_{\%}$ plane in which fifth and third-order models evolutions are in accordance or in contrast. The point 1 (ω_2=2500 rad/s, $\Delta V_{\%}$=0.05) belongs to the area in which both third and fifth-order model are stable, as demonstrated by the transients in Fig. 6. Then, the point 2 (ω_2=2500 rad/s, $\Delta V_{\%}$=0.035) is located in a zone in which

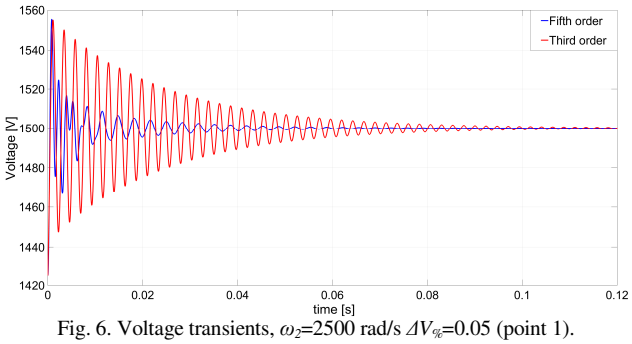

Fig. 6. Voltage transients, ω_2=2500 rad/s $\Delta V_{\%}$=0.05 (point 1).

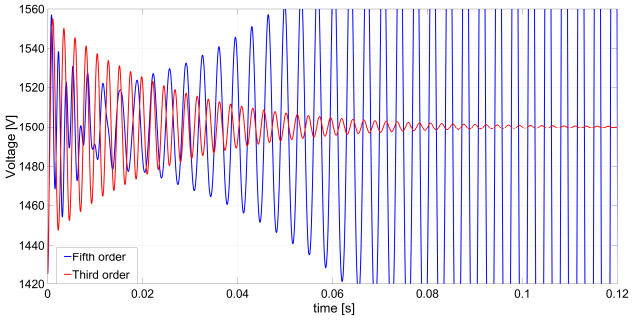

Fig. 7. Voltage transients, ω_2=2500 rad/s $\Delta V_{\%}$=0.035 (point 2).

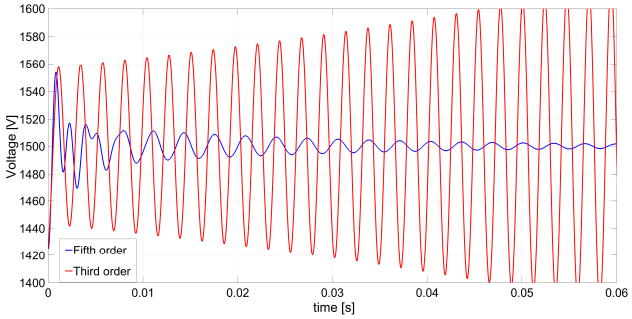

Fig. 8. Voltage transients, ω_2=2750 rad/s $\Delta V_{\%}$=0.06 (point 3).

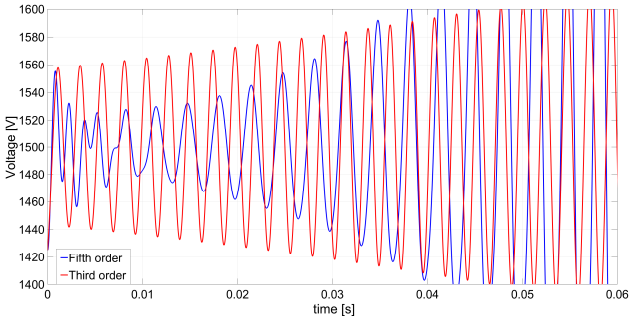

Fig. 9. Voltage transients, ω_2=2750 rad/s $\Delta V_{\%}$=0.04 (point 4).

the fifth-order model shows an unstable behavior, while the stability is ensured by the third-order model. Also these considerations are confirmed by the transients of Fig. 7. In this area, the third-order model cannot predict the stability performance of DC grid. Thus, the fifth-order one is here mandatory, as it performs closer to the real behavior of cascade-connected controlled systems. Other remarks in Fig. 8 by looking at point 3 (ω_2=2750 rad/s, $\Delta V_{\%}$=0.06), where the fifth-order model is still stable and the third one demonstrates an unstable evolution. Also in this case, the analytical study is validated. In the point 4 (ω_2=2750 rad/s, $\Delta V_{\%}$=0.04) third and fifth-order models perform again in accordance, showcasing the unstable evolution of Fig. 9. Also for this last point, the results in Fig. 5 are consistent.

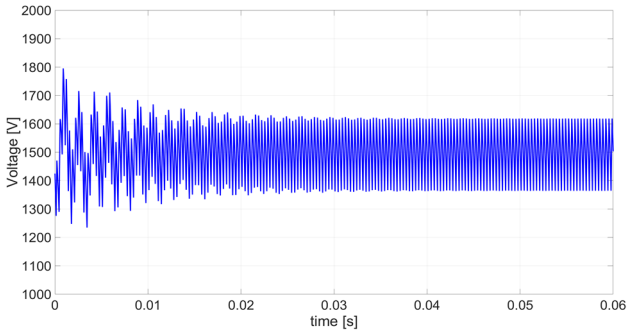

Fig. 10. Voltage transient, ω_2=1500 rad/s.

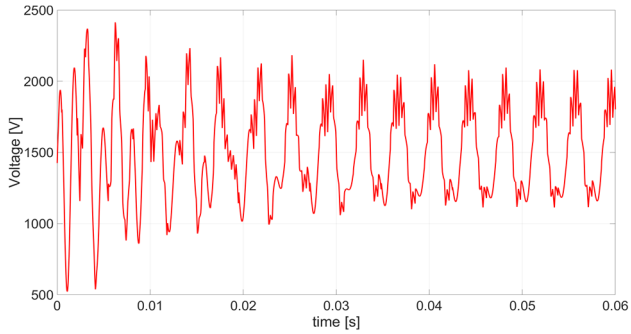

Fig. 11. Voltage transient, ω_2=2200 rad/s.

Finally, some Typhoon HIL circuital emulations are executed to further verify the mathematical conclusions. For this HIL test, two new crossing points are selected in Fig. 5, assuming a voltage ripple of 3% and two control bandwidths, 1500 rad/s (stable case, S) and 2200 rad/s (unstable case, U). The tests performed on HIL are similar to the ones made on AVMs. The dynamics transients confirm what is foreseen in Fig. 5. The Fig. 10 depicts the stable evolution for the control bandwidth of 1500 rad/s, while the evolution with the control bandwidth of 2200 rad/s results out of control as in Fig. 11. Evidently, this large variation in voltage activates the protection trip.

C. *Final conclusions*

The stability study in Fig. 5 provides interesting results on order reduction and new stable cross in the filter design. The analysis confirms how the third-order model is effective for a large zone of superimposition (i.e. points like 1). Then, the study identifies a critical zone (i.e. points like 2), where third-order modeling is insufficient. In the zone of point 3, the fifth-order model opens new possibilities of stable designs. Finally, the unstable designs for the points like 4 is confirmed both by fifth and third-order model.

V. Conclusions

The stability issue in cascade-connected DC shipboard microgrids is debated in this work. The analytical definition of the stability boundary for the complete fifth-order model is deduced thanks to an extension of the R-H criterion. This boundary is compared to the one from third-order model to understand its range of applicability. The results from this study on cascaded-converters case are useful also for more complex multi-converter DC grid. Indeed, it is possible to use equivalents on generating and load side converters in order to reduce the initial system to a simplified cascade-connected one. The design methodology of this paper shows its effectiveness when sizing stable filtering solutions in the converter-based DC microgrids.

Acknowledgment

The authors wish to thank Prof. Giovanni Giadrossi for his valuable contribution. The authors would like to thank Typhoon HIL for providing the HIL platform used in the development of this research work.

References

[1] J. F. Hansen and F. Wendt, "History and State of the Art in Commercial Electric Ship Propulsion, Integrated Power Systems, and Future Trends," in *Proceedings of the IEEE*, vol. 103, no. 12, pp. 2229-2242, Dec. 2015.

[2] M. Banaei, M. Rafiei, J. Boudjadar and M. -H. Khooban, "A Comparative Analysis of Optimal Operation Scenarios in Hybrid Emission-Free Ferry Ships," in *IEEE Transactions on Transportation Electrification*, vol. 6, no. 1, pp. 318-333, March 2020.

[3] S. Fang, Y. Wang, B. Gou and Y. Xu, "Toward Future Green Maritime Transportation: An Overview of Seaport Microgrids and All-Electric Ships," in *IEEE Transactions on Vehicular Technology*, vol. 69, no. 1, pp. 207-219, Jan. 2020.

[4] U. Javaid, F. D. Freijedo, D. Dujic and W. van der Merwe, "MVDC supply technologies for marine electrical distribution systems," in *CPSS Transactions on Power Electronics and Applications*, vol. 3, no. 1, pp. 65-76, March 2018.

[5] F. Wang, Z. Zhang, T. Ericsen, R. Raju, R. Burgos and D. Boroyevich, "Advances in Power Conversion and Drives for Shipboard Systems," in *Proceedings of the IEEE*, vol. 103, no. 12, pp. 2285-2311, Dec. 2015.

[6] D. Kumar and F. Zare, "A Comprehensive Review of Maritime Microgrids: System Architectures, Energy Efficiency, Power Quality, and Regulations," in *IEEE Access*, vol. 7, pp. 67249-67277, 2019.

[7] L. Herrera, W. Zhang and J. Wang, "Stability Analysis and Controller Design of DC Microgrids With Constant Power Loads," in *IEEE Transactions on Smart Grid*, vol. 8, no. 2, pp. 881-888, March 2017.

[8] T. Dragičević, X. Lu, J. C. Vasquez and J. M. Guerrero, "DC Microgrids—Part I: A Review of Control Strategies and Stabilization Techniques," in *IEEE Transactions on Power Electronics*, vol. 31, no. 7, pp. 4876-4891, July 2016.

[9] A. Kwasinski and C. N. Onwuchekwa, "Dynamic Behavior and Stabilization of DC Microgrids With Instantaneous Constant-Power Loads," in *IEEE Transactions on Power Electronics*, vol. 26, no. 3, pp. 822-834, March 2011.

[10] D. Park and M. Zadeh, "Dynamic Modeling, Stability Analysis, and Power Management of Shipboard DC Hybrid Power Systems," in *IEEE Transactions on Transportation Electrification*, vol. 8, no. 1, pp. 225-238, March 2022.

[11] "IEEE Recommended Practice for 1 kV to 35 kV Medium-Voltage DC Power Systems on Ships," in *IEEE Std 1709-2018 (Revision of IEEE Std 1709-2010)* , vol., no., pp.1-54, 7 Dec. 2018.

[12] S. Pastore, D. Bosich and G. Sulligoi, "Analysis of small-signal voltage stability for a reduced-order cascade-connected MVDC power system," *Proc. IECON 2017 - 43rd Annual Conference of the IEEE Industrial Electronics Society*, 2017, pp. 6771-6776.

[13] A. Vicenzutti, D. Bosich, A. A. Tavagnutti and G. Sulligoi, "System Stability and Short Circuit Contribution as Discordant Targets in Cascade Connected DC Microgrids: a Design Procedure," *Proc. 2022 International Conference on Smart Energy Systems and Technologies (SEST)*, 2022, pp. 1-6.

[14] D. Bosich, G. Giadrossi, S. Pastore, and G. Sulligoi, "Weighted Bandwidth Method for Stability Assessment of Complex DC Power Systems on Ships," *Energies*, vol. 15, no. 1, p. 258, Dec. 2021.

[15] A. A. Tavagnutti, D. Bosich and G. Sulligoi, "Stability-Oriented Analysis of a DC Shipboard Zonal Distribution System," *Proc. 2022 IEEE Power & Energy Society General Meeting (PESGM)*, 2022, pp. 1-5.

[16] G. A. Korn, T. M. Korn, Mathematical Handbook for Scientist and Engineers, 2nd ed., McGraw Hill Book Company, 1961.

APPENDIX

The expression (A1) identifies the denominator of the $Y_1(s)=I_1(s)/E(s)$ admittance at the output of the generating converter 1 for the fifth order model (Fig. 1). The (A1) is then simplified as in (A2), the R-H criterion is then applied to this last expression.

$$DenY(s) = L_1L_2C_1C_2R_Ls^5 + L_1L_2C_1s^4 + (L_1C_1R_L + L_1D_2^2R_LC_2 + L_2\,C_2\,R_L)s^3 + (L_1C_1R_L\omega_2 + L_1D_2^2 + L_2)s^2 + (R_L - L_1D_2^2\omega_2)s + R_L\omega_2 \tag{A1}$$

$$s^5 + \frac{1}{R_LC_2}s^4 + \frac{L_1C_1+L_1C_2D_2^2+L_2C_2}{L_1C_1L_2C_2}s^3 + \frac{L_1D_2^2+L_2+L_1C_1R_L\omega_2}{L_1C_1L_2C_2R_L}s^2 + \frac{R_L-L_1D_2^2\omega_2}{L_1C_1L_2C_2R_L}s + \frac{\omega_2}{L_1C_1L_2C_2} = 0 \tag{A2}$$

The alternative formulation of the R-H criterion [16] states that all the roots of a real n[th]-degree equation (A3), have negative real parts if and only if this is true for the $(n-1)^{st}$-degree equation (A4). This theorem may be applied repeatedly. For the purposes of this work, it is sufficient to lower the degree of eq. (A2) to three, applying eq. (A4) twice. The alternative formulations states also that the number of roots with negative real parts is precisely equal to the number of negative multipliers $-a_0^{(j)}/a_1^{(j)}$ (j=1,…,n-1; $a_0^{(0)}=a_0>0, a_1^{(0)}=a_1$) encountered in successive applications of the theorem. This last part of the theorem is not used in this work. Once obtained the (A2) expression reduced counterpart (9), it is possible to apply the original formulation of the R-H criterion, thus identifying the conditions for system stability. Those conditions (10)-(14) are included in Section III, and the complete expression of $C_2^{\pm}$ is given in (A5).

$$f(x) = a_0x^n + a_1x^{n-1} + \cdots + a_{n-1}x + a_n = 0 \tag{A3}$$

$$a_0'x^{n-1} + a_1'x^{n-2} + \cdots = a_1x^{n-1} + a_2x^{n-2} + \cdots - \frac{a_0}{a_1}a_3x^{n-2} - \frac{a_0}{a_1}a_5x^{n-4} - \cdots = 0 \tag{A4}$$

$$C_2^{\pm} = \frac{R_L+\omega_2(L_2-D_2^2L_1)+R_L(1-\omega_2^2L_1C_1)\pm\sqrt{\left[-R_L+\omega_2(L_2-D_2^2L_1)+R_L(1-\omega_2^2L_1C_1)\right]^2+4\omega_2^2L_2D_2^2L_1}}{2R_L^2\omega_2} \tag{A5}$$